A phase field approach for bone remodeling based on a second-gradient model

J.F. Ganghoffer, R. Rahouadj, Julien Boisse, J. Schiavi

Version of Record: https://www.sciencedirect.com/science/article/pii/S0093641319300448
Manuscript_a3274b6f3582d4052d137f8111835d2e

A phase field approach for bone remodeling based on a second-gradient model

J.F. Ganghoffer[(1)], R. Rahouadj[(1)], J. Boisse[(2)], J. Schiavi [(3)]

[(1)] LEM3, Université de Lorraine, UMR CNRS 7239, 7, rue Félix Savart. 57073 Metz Cedex, France
[(2)] LEMTA, Université de Lorraine, UMR CNRS 7563, 2, Avenue de la Forêt de Haye. 54500 Vandœuvre, France
[(3)] Mechanobiology and Medical Device Research Group (MMDRG), Biomechanics Research Centre (BioMEC), Biomedical Engineering, National University of Ireland Galway, Galway, Republic of Ireland

Abstract. A mechanobiological model of bone remodeling is developed involving mineralization in a moving diffuse interface separating the marrow containing the bone cells responsible for the remodeling from the newly formed bone. A scalar phase field quantifies the degree of mineralization within the interface at the level of the bone microstructure, varying continuously between the nil lower value (no mineral) and unity for the fully mineralized phase corresponding to new bone. The field equations for the mechanical, chemical, and interfacial phenomena are written under the umbrella of thermodynamics of irreversible processes. A strain gradient model is developed to account for the impact of the underlying hierarchical microstructure on the effective response of bone. Second gradient terms are motivated by the high strain and stress concentrations close to defects, both at mesoscopic and microscopic scales. The combination of the balance equations for the microforce associated to the phase field and the kinetic equations lead to the Ginzburg–Landau equation for by the phase field with a source term accounting for the dissipative microforce.

Keywords: bone remodeling; phase field; diffuse interface; strain gradient effects; Ginzburg-Landau equation

1. Introduction

Bone microstructure is organized hierarchically to response to the demand of resistance to bending and strain applied on the skeleton (fig. 1).

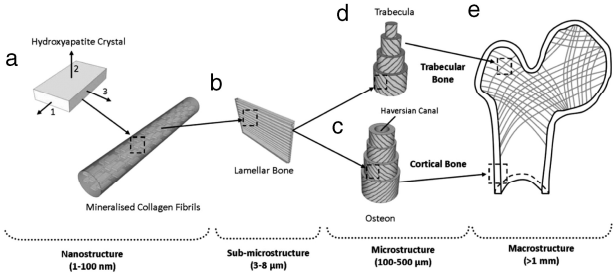

Figure 1: Hierarchical structure of bone from the nanoscale of the collagen and hydroxyapatite phases to the macroscale of osteons forming compact bone (Vaughan et al., 2012).

This architecture provides a high resistance to fracture and contributes to limit and stabilize microcracks which are stopped for 60 % by the osteon (Bertram and Biewener, 1988; O'Brien et al. 2005). Bone is an organized mesh of collagen fibers and others non-collagenous proteins where hydroxyapatite crystals are forming to provide to the tissue its strength. The assemblage of ECM (the extracellular matrix) forms a lamellar bone structure where osteocytes are embedded and their assemblage forms the osteons. Within cortical bone these cylindrical structures are several millimeters long and around 0.2 mm in diameter. They are enclosed by a boundary called the cement line, a compliant interface responsible for a contrast in stiffness between osteons and bone (fig. 1). The bone remodeling is a cyclic adaptation process in response to variations in external loads and biochemical factors, involves three types of bone cells: osteoclasts, which resorb the old or damaged bone. Osteoblasts, which form new bone in the second phase; osteocytes, which are mechanosensing cells and formed an interconnected network that can be disrupted by microcracks. Osteocytes are inducing mechanotransduction pathways and orchestrate bone homeostasis (Parfitt, 1994; Sommerfeldt and Rubin, 2001). At the end of the remodeling process bone mineralization occurs in the diffuse interface separating the marrow from new bone (fig. 2). The interface thickness is of the order of 5.10^{-4} m (Ganghoffer et al., 2016).

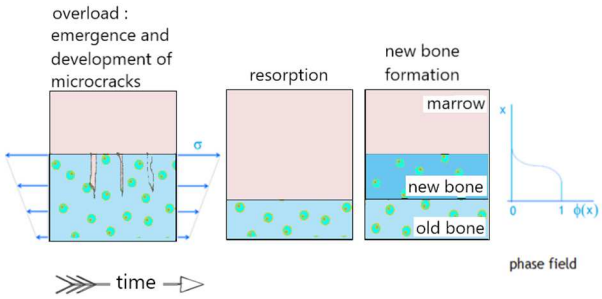

Figure 2: Schematic remodeling cycle including 4 main steps: healthy bone, initiation and development of damage (microcracks) under mechanical stresses, resorption, and new bone formation. The phase order parameter is represented in 1D as a function of spatial position x.

Bone tissue is morphologically separated from the marrow by the bone lining cells for both cortical and trabecular bone. Works in the literature show that substantial size effects occur in the elastic behavior of bones at different levels of its ultrastructure and microstructure, namely at the scale of single osteons (Lakes, 1995), human compact bone (Frasca et al., 1981; Yang and Lakes, 1981, 1982; Park and Lakes, 1986; Buechner and Lakes, 2003), and human trabecular bone (Harrigan et al., 1988; Ramezani et al., 2012). Size effects in osteons are caused by the compliant response of the interfaces between laminae that are responsible for bending (fig. 1). Since these hierarchical architectures are structurally inhomogeneous and show strong contrast in properties, they generate strain and stress internal gradients. The bone tissue stiffness is strongly dependent on the degree of mineralization (van der Linden et al., 2001; van Eijden et al., 2004). Furthermore, since strain

gradients develop in inverse proportion of size, this entails that they can be small at the macrolevel although much larger at small scales, thus they would dominate the mechanical response and have a strong influence on coupled multiphysical phenomena. The presence of a strong texture within bones together with its inhomogeneous structures exhibiting radial porosity gradients and curved walls of the osteons that form tubular structures with concentric lamellae (fig. 1) enhances the strain gradients. In trabecular bone as well, the mechanical properties at continuum level vary by about 30% over a distance that spans three to five trabeculae thus requiring using enhanced continuum theories (Harrigan et al., 1988). It is therefore important to include these strain gradients into the formulation of a description of bone remodeling and as a possible trigger of the cell activity responsible for bone remodeling and bone growth.

Surface and interface effects present in bone can be modeled in the framework of second-gradient theories of elasticity in line with the seminal work of Mindlin (1964), see (Eremeyev, 2015) and references therein. In particular, second-gradient theories were developed for porous media like bone for which surface effects play a crucial role (Sciarra et al., 2007), and more recently in Giorgio et al. (2017), who proposed an approach including the porosity as an additional relevant microstructural variable. In contrast to these works, we shall develop a model at the scale of individual trabeculae in order to model the evolution of the interface between the marrow phase and newly apposed bone.

Surface effects (the sealing zone at the boundary of a single trabeculae or the cement line enclosing osteons) are able to predict the size effects observed for nanosized materials (Wang et al., 2006). Gurtin and Murdoch (1975a, b) model for surface effects was generalized in Steigmann and Ogden (1997, 1999) to account for the bending stiffness of the surface layer. Recent work based on numerical simulations and a regression analysis (Webster et al., 2015) further indicate that the amount of resorbed bone is strongly correlated to the gradients of the strain energy density in the marrow and to the strain gradients within the trabecular matrix. Strong strain gradients may develop for instance at the interface between bone and an implant, but they in fact develop over the different imbricated scales up to the macroscopic bone level, due to the existence of defects (cavities, microcracks, localized damage zones), the strong contrast of properties between hard (mineralized bone) and soft components (the marrow phase).

Our modeling scale is that of a window of analysis like the one shown on the left insert of Fig. 2, including microcracks generating high internal strain gradients, the marrow phase, the existing bone substrate and newly apposed bone. Phase field models have proven to be efficient in modeling the motion of interfaces and the growth of precipitates relying on a thermodynamic formulation including non-convex free energy potentials (Ammar et al., 2009; Forest et al, 2011) and references therein. The description of biological phenomena with the phase field approach is seemingly relatively new, especially in the field of bone remodeling. We incorporate as a novel aspect strain gradients into a (strain gradient) elastic constitutive model, wherein the effective first and second gradient mechanical properties will be modulated by the phase field variable. The diffuse interface between the marrow phase and the newly formed mineral witnesses strong deformation gradients due to the continuous change of mineral composition which makes the interface a graded material, the mechanical properties of which varying across the thickness.

2. Phase field modeling: balance equations

The degrees of freedom (DOFs) of the thermodynamic system consisting of a microvolume of cortical bone including microcracks and the marrow phase (fig. 1) includes the order parameter ϕ representing the phase field, its gradient $\nabla\phi$, the first gradient of the displacement $\mathbf{u}$, the strain gradient tensor $\boldsymbol{\varepsilon}\otimes\nabla$, the total number of moles k-species n_k and the absolute temperature T; these variables are encapsulated into the vector of DOF's $\{\phi, \nabla\phi, \mathbf{u}\otimes\nabla, \boldsymbol{\varepsilon}\otimes\nabla, T\}$. The phase field describes the degree of mineralization of the diffuse interface; it varies continuously between the lower value (no mineral) and unity (fully mineralized phase, e.g. new bone), allowing the consideration of a diffuse moving interface, Fig. 2. The gradient of the phase field rapidly varies in the diffuse interface between bone and marrow or due to the contrast of properties of the ultrastructure and it contributes to the corresponding interface energy.

2.1. Strain gradient kinematics

We define the first and second order kinematics over the composite domain made of the mineral and collagen fibers, adopting reasonably a small strains framework (maximum bone strains are of the order of 0.3% (Martin et al., 1998): the first and second gradient tensors $\boldsymbol{\varepsilon}(\mathbf{x})$ and $\mathbf{k}(\mathbf{x})$ are defined as follows:

$$\boldsymbol{\varepsilon}(\mathbf{x}) := \frac{1}{2}\left(\mathbf{U}(\mathbf{x})\otimes\nabla + \mathbf{U}(\mathbf{x})\otimes\nabla^{T}\right) \rightarrow \varepsilon_{ij} = \varepsilon_{ji},$$
$$\mathbf{k}(\mathbf{x}) := \boldsymbol{\varepsilon}(\mathbf{x})\otimes\nabla \rightarrow k_{ijk} = k_{jik} \quad (1)$$

The kinematics is defined at the mesoscopic scale (including few lamellae for osteons) representing a small volume element including a microstructure within which remodeling phenomena occur. It makes then sense to define growth strains and second gradient of growth tensors representing the irreversible 'deformation' due to the bone mass production and internal microstructure evolution. These mappings are in general non compatible, so they are accompanied by elastic mappings; this entails the following additive split of the total strain and strain rate tensors (time and space derivation commute):

$$\boldsymbol{\varepsilon} = \boldsymbol{\varepsilon}_g + \boldsymbol{\varepsilon}_e \;\Rightarrow\; \dot{\boldsymbol{\varepsilon}} = \dot{\boldsymbol{\varepsilon}}_g + \dot{\boldsymbol{\varepsilon}}_e \quad (2)$$

with $\boldsymbol{\varepsilon}_g, \boldsymbol{\varepsilon}_e$ successively the growth and elastic mapping. The elastic 'strain', tensor $\boldsymbol{\varepsilon}_e$ in (2), may have one chemical origin (hydrostatic term due to chemical reactions, thus associated to the phase field itself representing the degree of mineralization) and the accommodation of defects, especially in the vicinity of microcracks (a non-hydrostatic contribution), this last contribution fading with ongoing remodeling. At the scale of the RVE shown in fig. 2 for cortical bone and considering that remodeling occurs by apposition of mineral, it is accordingly a surface growth process described by a surface growth velocity field $\mathbf{V}_g$ (over the RVE boundary); in analogy with the equality, $\int_V \mathrm{grad}\mathbf{V}\,dX = \int_{\partial V} \mathbf{V}\otimes\mathbf{N}\,dS$, with $\mathbf{N}$ the unit exterior normal to

the volume boundary ∂V, the average growth velocity gradient $\mathbf{L}_g$ and its symmetrical part can be elaborated as the following surface integral

$$\mathbf{L}_g := \frac{1}{|\Omega_g|}\int_{\partial\Omega_g} \mathbf{V}_g \otimes \mathbf{N} dS \Rightarrow$$
$$\mathbf{D}_{lg} := \frac{1}{2}\left(\mathbf{L}_g + \mathbf{L}_g^{\,T}\right) = \frac{1}{|\Omega_g|}\int_{\partial\Omega_g} \frac{1}{2}\left(\mathbf{V}_g \otimes \mathbf{N} + \mathbf{N} \otimes \mathbf{V}_g\right) dS \cong \dot{\boldsymbol{\varepsilon}}_g \quad (3)$$

with $\mathbf{N}$ the unit exterior normal to the boundary of $|\Omega_g|$, the RVE volume isolated in fig. 2, including a substructure made of a set of lamellae within cortical bone and micro defects like microcracks, voids, microdamage. Note that the growth 'strain' appears as a result of averaging microstructural evolutions, especially the surface evolution due to the apposition of mineral. Surface remodeling is here deemed as fully irreversible, so that the surface remodeling field is compatible. The last equality follows from the small strains rate assumption due to bone growth being a slow process (the remodeling cycle lasts about 3 weeks). Due to this, one can further linearize the average strain rates and approximate them by their small strains rate counterparts (times derivatives and spatial derivatives commute): it thus holds the following approximations:

$$\mathbf{D} \cong \dot{\boldsymbol{\varepsilon}}, \mathbf{D}_g \cong \dot{\boldsymbol{\varepsilon}}_{lg} \cong \mathbf{D}_e \cong \dot{\boldsymbol{\varepsilon}}_{le} = \dot{\boldsymbol{\varepsilon}} - \dot{\boldsymbol{\varepsilon}}_{lg} \quad (4)$$

Turning now to the second order average kinematics, the average second gradient rate of growth can be constructed as the following third order tensor defined by a surface averaging over the RVE:

$$\dot{\mathbf{k}}_g := \frac{1}{|V|}\int_{\partial V_B} \left(\mathbf{V}_g \otimes \nabla_x\right) \otimes \mathbf{N} dS \equiv$$
$$\frac{1}{|V|}\int_{V_B} \left(\mathbf{V}_g \otimes \nabla_x\right) \otimes \nabla_x dV \to \left(\dot{\mathbf{k}}_g\right)_{ijk} = \left(\dot{\mathbf{k}}_g\right)_{ikj} \quad (5)$$

Recent works tend to prove the importance of curvature effects at the macroscopic level (Nowak et al., 2018). It is especially in line with the idea that surface remodeling will act to minimize stress gradients on the surface of either trabeculae or at the level of the outer boundary of a macroscopic bone sample.

The second gradient elastic rate of deformation tensor is then elaborated as the difference between the total second gradient rate of deformation tensor and the (second gradient) rate of growth,

$$\mathbf{D}_{2e} \cong: \dot{\mathbf{k}}_e = \dot{\boldsymbol{\varepsilon}} \otimes \nabla - \dot{\mathbf{k}}_g \quad (6)$$

wherein we have used the small strain rate assumption for the first equality (the subscript 2 in any tensor therein indicates a third order tensor representative of second gradient effects):

This additive decomposition of second gradient rates of deformation directly entails by time integration the additive decomposition of the strain gradient tensor:

$$\mathbf{k} = \mathbf{k}_e + \mathbf{k}_g \quad (7)$$

The irreversible contribution $\mathbf{k}_g$ may be also caused by damage like defects that are prone to strong spatial gradients, especially in the vicinity of interfaces or close to the microcrack tips, thus it could itself split into a defect part and a phase term. The total number of moles n_k results from the production of the corresponding chemical species by chemical reactions n_k^{prod} and of exchanges with the external environment n_k^{exch} - in the present case the bone marrow - as expressed in the balance law

$$n_k = n_k^{exch} + n_k^{prod} \quad (8)$$

The principle of virtual power states that the sum of the virtual power of internal, external and contact forces vanishes in a quasi-static situation, so that it holds the equality

$$\int_V p^{(i)} dV + \int_V p^{(e)} dV + \int_{\partial V} p^{(c)} dS = 0 \quad (9)$$

The internal power of mechanical forces includes a contribution from the strain and the strain gradients; a proper form of the second gradient growth model is obtained from the expression of the local dissipation reflected by Clausius-Duhem inequality, adopting the framework of generalized standard materials. The effective material is characterized by a free energy density sum of elastic and growth contributions, each of them depending on the average first and second gradient of the elastic and growth deformation tensors

$$\psi = \psi_e\left(\boldsymbol{\varepsilon}_e, \mathbf{k}_e\right) + \psi_g\left(\boldsymbol{\varepsilon}_g, \mathbf{k}_g\right) \quad (10)$$

Note that the growth deformations are here considered as internal variables associated to a purely dissipative behavior. Using the additive split of the strain rate tensor in (2) and (7), the virtual power of internal forces writes after elementary calculations due to the introduced additive split of the average strain rates as

$$p_{i,mech} = -\boldsymbol{\sigma} : \dot{\boldsymbol{\varepsilon}}_e - \boldsymbol{\sigma} : \dot{\boldsymbol{\varepsilon}}_g - \mathbf{S} \therefore \dot{\mathbf{k}}_e - \mathbf{S} \therefore \dot{\mathbf{k}}_g \quad (11)$$

with $\boldsymbol{\sigma}, \mathbf{S}$ the Cauchy stress and hyperstress tensors, respectively a second order and a third order tensor. The hyperstress represents the internal moments of Cauchy stress with respect to a fixed point (the center of the RVE). The virtual power of external forces for the strain gradient continuum includes successively volumetric, surface, line and edge contributions:

$$\delta W_{mech,ext} = \int_V f_k \delta u_k dV + \int_S T_k \delta u_k dS + \int_S R_k D\delta u_k dS + \int_C E_k \delta u_k dS \quad (12)$$

The quantities T_k, R_k, E_k therein are respectively the surface tractions, the surface double tractions and the edge tractions; the quantity $D\delta u_k$ in (12) represents the normal derivative of the variation δu_k. The balance of linear momentum writes successively in tensor and index notation:

$$\mathrm{div}\left(\boldsymbol{\sigma} - \mathrm{div}(\mathbf{S})\right) + \mathbf{f} = \mathbf{0} \leftrightarrow \left(\sigma_{ij} - S_{ijk,k}\right)_{,j} + f_i = 0 \quad (13)$$

Classical derivations lead to the identification of the external forces versus Cauchy stress and hyperstress (the double bracket $[\![.]\!]$ stands for the jump of the enclosed quantity) as

$$P_k = n_j\left(\sigma_{jk} - S_{ijk,i}\right) - D_j\left(n_i S_{ijk}\right) + \left(D_l n_l\right) n_j n_i S_{ijk},$$
$$R_k = n_i n_j S_{ijk}, E_k = s_m e_{mlj} [\![n_l n_j S_{ijk}]\!] \quad (14)$$

with e_{mlj} the components of the third order permutation tensor, and s_m the components of the surface vector. The occurrence of these forces involving contributions specific to second gradient continua leads to specific features like boundary layers and concentrated forces.

Summarizing, the virtual power of internal, external and contact forces writes (Ganghoffer et al., 2016):

$$p^{(i)} = \pi_\phi \dot{\phi} - \xi_\Phi . \nabla\dot{\phi} - \boldsymbol{\sigma} : \mathbf{u} \bar{\otimes} \nabla - \mathbf{S} \therefore \dot{\boldsymbol{\varepsilon}} \otimes \nabla + \mu_k^{prod} \dot{n}_k^{prod} \quad (15)$$

$$p^{(e)} = \pi_\phi^{ext} \dot{\phi} + \mathbf{f} . \dot{\mathbf{u}} + \mu_k^{prod\ ext} \dot{n}_k^{prod} \quad (16)$$

$$p^{(c)} = \pi_\phi^{cont} \dot{\phi} + \mathbf{t} . \dot{\mathbf{u}} + \mathbf{R} . D_n \mathbf{u} + \mu_k^{prod\ cont} \dot{n}_k^{prod} \quad (17)$$

with π_ϕ, π_ϕ^{ext}, π_ϕ^{cont} therein representing the internal, external and contact forces associated to ϕ respectively, ξ_Φ the microforce associated to $\nabla\phi$, $\boldsymbol{\sigma}$ the (second order) Cauchy stress tensor, and $\mathbf{S}$ the hyperstress third order tensor. The notation $D_n\mathbf{u}$ stands for the normal derivative. The scalars μ_k^{prod}, $\mu_k^{prod\,ext}$, $\mu_k^{prod\,cont}$ therabove are the chemical potentials (for the production, external and contact chemical actions respectively) associated to the production term n_k^{prod} and f, T, R terms in '16), (17) denote the volume and surface densities of external forces. The free energy may be expressed as $\Psi\left(\phi, \nabla\phi, \boldsymbol{\varepsilon}^e, \mathbf{k}^e, n_k^{exch}, T\right)$, where ε^e, k^e are respectively the elastic part of the total and elastic strain; in analogy with mechanics, the free energy density incorporates the number of moles being exchanged. The equilibrium equations and associated boundary conditions arising from the principle of virtual power are of the following local form in V ($\mathbf{f}$ is the body force vector):

$$(\boldsymbol{\sigma} - \mathbf{S}.\nabla).\nabla + \mathbf{f} = 0, \quad (\boldsymbol{\sigma} - \mathbf{S}.\nabla).\mathbf{n} = \mathbf{T}$$
$$\nabla.\xi_\Phi + \pi_\phi^{ext} + \pi_\phi = 0, \ \xi_\Phi.\mathbf{n} = \pi_\phi^{cont}$$
$$(\mu_k^{prod} + \mu_k^{prod\,ext})\,\dot{n}_k^{prod} = 0 \qquad (18)$$

the decomposition of the mole fraction of k-species into exchanged and produced terms, viz $\dot{n}_k = \dot{n}_k^{exch} + \dot{n}_k^{prod}$, which implies the condition $\mu_k^{prod\,cont}\,\dot{n}_k^{prod} = 0$, together with the boundary conditions on ∂V for the stress field and the microforce. We further assume $\pi_\phi^{ext} = 0$.

3. Phase field model of bone remodeling in the context of strain gradient mechanics and TIP

The thermodynamics of irreversible processes (TIP) is the adequate framework to express the internal dissipation accounting for the multiphysical processes underlying bone remodeling. The combination of the first principle and the virtual power principle leads to the energy balance based on free energy:

$$\dot{\Psi} = \partial_\phi\Psi\,\dot{\phi} + \partial_{\nabla\phi}\Psi.\nabla\dot{\phi} + \partial_{\varepsilon^e}\Psi : \dot{\varepsilon}^e + \partial_{k^e}\Psi \therefore \dot{k}^e + \partial_{n_k^{exch}}\Psi\,\dot{n}_k^{exch} + \partial_T\Psi\,\dot{T} \qquad (19)$$

$$\dot{E} = -P^{(i)} + \delta Q \qquad (20)$$

$$\dot{e} = -\pi_\phi\dot{\phi} + \xi_\Phi.\nabla\dot{\phi} + \boldsymbol{\sigma}:\mathbf{u}\otimes\nabla - \mathbf{S}\therefore\boldsymbol{\varepsilon}\otimes\nabla - \mu_k^{prod}\,\dot{n}_k^{prod} - \nabla.\mathbf{q} \qquad (21)$$

$$T\dot{s} = \dot{e} - \dot{T}s - \dot{\Psi} \qquad (22)$$

In (20), the scalar quantities $\dot{E}, P^{(i)}, \delta Q$ denote successively the rate of the total internal energy, the internal power of forces and the total amount of heat. Quantities $e, s,$ in (22) are successively the internal energy and entropy density. Last expression combined with the second principle, inequality

$$\dot{s} \geq -\nabla.\left(\frac{q}{T}\right) + \frac{1}{T}\nabla.\left(\mu_k^{prod}J_k\right) \qquad (23)$$

leads in a straightforward manner to Clausius-Duhem inequality, which leads following the standard Coleman-Noll procedure to the state laws and the residual dissipation, this last quantity taking the form

$$-\pi_\phi^{diss}\,\dot{\phi} + \boldsymbol{\sigma} : \dot{\boldsymbol{\varepsilon}}^{irr} + \mathbf{S}\therefore\dot{\mathbf{k}}^{irr} - \mu_k^{prod}\,\dot{n}_k^{prod} - J_k.\nabla\mu_k^{prod} - \left(\frac{1}{T}\right)q.\nabla T \geq 0 \qquad (24)$$

Previous inequality entails the different sources of dissipation associated with the phase field, mechanical, chemical and thermal phenomena, successively specified as:

$$D_\phi = -\pi_\phi^{diss}\,\dot{\phi} \quad , D_{mech} = \boldsymbol{\sigma} : \dot{\boldsymbol{\varepsilon}}^{irr} + \mathbf{S}\therefore\dot{\mathbf{k}}^{irr},$$
$$D_{chem} = -\mu_k^{prod}\,\dot{n}_k^{prod} - J_k.\nabla\mu_k^{prod}, D_{therm} = -q.\left(\frac{\nabla T}{T}\right) \qquad (25)$$

One needs in order to complete the thermodynamic model to specify the kinetic laws governing the evolution of the internal variables. In view of this objective, we introduce the dissipation function $\Omega\left(\pi_\phi^{diss}, \sigma, S, \nabla\mu_k^{prod}, \mu_k^{prod}, \nabla T\right)$ decomposing into different contributions involving the forces satisfying the previous state laws,

$$\Omega = \frac{1}{2}L(\phi)\,\nabla\mu_k^{prod}.\nabla\mu_k^{prod} - \frac{1}{2}\left(\frac{1}{\tau_\phi}\right)\left(\pi_\phi^{diss}\right)^2 + f(\boldsymbol{\sigma}, \mathbf{S}) - \frac{1}{2}\left(\frac{1}{\tau_k}\right)\left(\mu_\phi^{prod}\right)^2 + \frac{1}{2}k\left(\frac{\nabla T}{T}\right)^2 \qquad (26)$$

satisfying Onsager's properties, and with the dissipative microforce, Cauchy stress (a second order tensor), the third order hyperstress tensors, the chemical potential and entropy density successively given by

$$\pi_\phi^{diss} = \pi_\phi + \partial_\phi\Psi, \boldsymbol{\sigma} = \partial_{\varepsilon^e}\Psi, \mathbf{S} = \partial_{k^e}\Psi,$$
$$\mu_k^{prod} = \partial_{n_k^{exch}}\Psi, s = -\partial_T\Psi \qquad (27)$$

In (26), the yield function $f(\boldsymbol{\sigma}, \mathbf{S})$ depends on both the stress and hyperstress tensors. As expected, the resulting kinetic laws follow from previous writing as

$$\dot{\boldsymbol{\varepsilon}}_{mech}^{irr} = \frac{\partial\Omega}{\partial\sigma} = \frac{\partial f}{\partial\sigma}, \dot{\mathbf{k}}_{mech}^{irr} = \frac{\partial\Omega}{\partial S} = \frac{\partial f}{\partial S}, \dot{\phi} = -\frac{\partial\Omega}{\partial\pi_\phi^{diss}} = -\frac{1}{\tau_\phi}\pi_\phi^{diss}$$
$$\dot{n}_k^{prod} = \frac{\partial\Omega}{\partial\mu_k^{prod}} = -\frac{1}{\tau_k}\mu_k^{prod}, -\mathbf{J}_k = \frac{\partial\Omega}{\partial\nabla\mu_k^{prod}} = L(\phi)\,\nabla\mu_k^{prod} \qquad (28)$$

The influence function $L(\phi)$ is taken as in (Ganghoffer et al., 2016)

$$L(\phi) = h(\phi)\,D_B\ /k_B + \left(1 - h(\phi)\right)D_M\ /k_M, h(\phi) = \phi^2(3 - 2\phi) \qquad (29)$$

The scalars D_B, D_M in (29) represent the diffusivities within bone or marrow respectively, and the Fick's law is recovered in both phases. These equations successively express the evolution of the irreversible mechanical strain tensor, of the phase field, the number of produced moles, and the flux of chemical species. Combining the balance equations (18) with the state equation delivers the so-called Ginzburg-Landau equation governing the spatio-temporal evolution of the phase field

$$\nabla.\frac{\partial\Psi}{\partial\nabla\phi} - \left(\frac{\partial\Psi}{\partial\phi}\right) = -\pi_\phi^{diss} \qquad (30)$$

The balance laws of forces and microforces, the state laws and the kinetic equations define the set of equations one has to solve in order to describe the formation of new bone through the evolution of the interface between the apposed bone and the marrow.

One may consider in line with the small strains and strain rates context the usual additive decomposition of the total strain rate and its gradients into mechanical and chemical sources of dissipation

$$\dot{\boldsymbol{\varepsilon}}^{irr} = \dot{\boldsymbol{\varepsilon}}_{mech}^{irr} + \dot{\boldsymbol{\varepsilon}}_{prod}^{irr}, \dot{\mathbf{k}}^{irr} = \dot{\mathbf{k}}_{mech}^{irr} + \dot{\mathbf{k}}_{prod}^{irr} \qquad (31)$$

The high local strains in the vicinity of microcracks leads to a local plastic deformation of the mineral phase. The existence of strain gradients reflects the continuous change of mineral content across the diffuse interface. The elastic strain rate and elastic strain rate gradient are then computed as the differences involving the first and second gradient compliance tensors $\mathbf{S}, \mathbf{D}$:

$$\dot{\boldsymbol{\varepsilon}}^{e} = \dot{\boldsymbol{\varepsilon}} - \dot{\boldsymbol{\varepsilon}}^{irr} = \mathbf{S} : \dot{\boldsymbol{\sigma}},\ \dot{\mathbf{k}}^{e} = \dot{\mathbf{k}} - \dot{\mathbf{k}}^{irr} + \mathbf{D} \therefore \dot{\mathbf{S}} \quad (32)$$

We next assume that the irreversible strain rate linked to the production of hydrostatic k-species is an isotropic tensor linearly depending on the rate of produced species; furthermore, the irreversible rate of strain gradient is assumed to be oriented along the gradient $\vec{\nabla} \dot{n}_k^{prod}$, so that it holds

$$\dot{\boldsymbol{\varepsilon}}_{prod}^{irr} = \gamma\, \dot{n}_k^{prod}\, \mathbf{I}, \dot{\mathbf{k}}_{prod}^{irr} = \delta\, \vec{\nabla} \dot{n}_k^{prod} \otimes \mathbf{I} \quad (33)$$

where $\mathbf{I}$ represents the second order identity tensor. Furthermore, the production of species-k is directly correlated to the change of the order parameter reflecting the formation of new bone

$$\dot{n}_k^{prod} = a\, \dot{\phi},\ \text{thus}\ \nabla \dot{n}_k^{prod} = a \nabla\, \dot{\phi} \quad (34)$$

These two assumptions lead to the following relations for the chemical irreversible strains and strain gradients versus the phase field rate and rate of gradient:

$$\dot{\boldsymbol{\varepsilon}}_{prod}^{irr} = a\, \gamma\, \dot{\phi}\, \mathbf{I},\ \dot{\mathbf{k}}_{prod}^{irr} = b \delta\, \vec{\nabla} \dot{\phi} \otimes \mathbf{I} \quad (35)$$

Similarly, the irreversible strain gradient rate (a third order tensor) is assumed to be linked to the gradient of the rate of produced species, in the form $\dot{\mathbf{k}}_{prod}^{irr} = \delta \nabla\, \dot{n}_k^{prod} \otimes \mathbf{I}$. Last relation means that the trace of $\dot{\mathbf{k}}_{prod}^{irr}$ is the vector defined from the gradient of $\dot{n}_k^{prod}$, supposed to be oriented essentially in the direction of the normal to the interface. This leads to the following expression of the elastic strain rate and rate of elastic strain gradient

$$\dot{\boldsymbol{\varepsilon}}^{e} = \dot{\boldsymbol{\varepsilon}} - a\, \gamma\, \dot{\phi}\, \mathbf{I} - \frac{\partial f}{\partial \sigma}, \dot{\mathbf{k}}^{e} = \dot{k} - a\ \delta \otimes \nabla\, \dot{\phi}\, \mathbf{I} - \frac{\partial f}{\partial S} \quad (36)$$

The free energy taking into account the chemical and mechanical contributions expresses as

$$\Psi\left(\phi, \nabla\phi, \boldsymbol{\varepsilon}^{e}, \mathbf{k}^{e}, n_k^{exch}, T\right) = \Psi_{mech}(\boldsymbol{\varepsilon}^{e}, \mathbf{k}^{e}, \phi, T) + \Psi_{chem}\left(n_k^{exch}, \phi, \nabla\phi\right) \quad (37)$$

with the mechanical and chemical contributions therein, quantities $\Psi_{mech}(\varepsilon^{e}, k^{e}, \phi, T)$ and $\Psi_{chem}\left(n_k^{exch}, \phi, \nabla\phi\right)$ respectively. Regarding mechanical aspects, the mechanical free energy reads

$$\Psi_{mech}(\varepsilon^{e}, k^{e}, \phi, T) = \frac{1}{2}\varepsilon^{e} : C(\phi, T) : \varepsilon^{e} + \frac{1}{2} k^{e} : A(\phi, T) : k^{e} \quad (38)$$

with $C(\phi, T), A(\phi, T)$ therein the first and second gradient elastic stiffness tensors, depending on the order parameter ϕ, and upon the elastic properties of the medium. A mixture law is used including the interpolation function $h(\phi)$, involving the first and second gradient elasticity tensors C_B, A_B, C_M, A_M of the new bone and marrow respectively (the same interpolation function $h(\phi)$ is here selected for both first and second gradient rigidity tensors). The chemical energy term is chosen as in (Ganghoffer et al., 2016). We obtain following the same method as in (Ganghoffer et al., 2016) the spatio-temporal evolution of the phase field, the following parabolic equation involving mechanical and chemical energies in the bracket term:

$$\tau_\phi\, \dot{\phi} = \alpha \Delta\phi + 2\phi\,(1-\phi)(2\phi - 1)W + 6\phi\,(1-\phi)\left[-\frac{1}{2}\boldsymbol{\varepsilon}^{e} : (C_B - C_M) : \boldsymbol{\varepsilon}^{e} - \frac{1}{2}\mathbf{k}^{e} \therefore A_B \therefore \mathbf{k}^{e} + (\Psi_M - \Psi_B)\right] \quad (39)$$

The scalar parameters W and α control the diffuse interfaces behavior. Given a chemical free energy of the type "$W\phi^2(1-\phi)^2 + \frac{\alpha}{2}\nabla\phi.\nabla\phi$" and a planar interface at equilibrium, the diffuse interface width can be estimated as $\delta \cong 2\sqrt{2\alpha/W}$, with the parameter α therein quantifying the strength of interfacial effects. The marrow phase is deemed to follow a pure first gradient elastic behavior. The network of osteocytes detects microcracks and local damages, which naturally involves high local strains and strain gradients close to zones of ultimate strength, so that the material locally deforms plastically. The irreversible mechanical strain and strain gradient associated to the development of the plastic zone can be computed from a generalized Von Mises yield criterion including both stress and hyperstress tensors; this is however outside the scope of this contribution.

4. One dimension example: bone representative unit cell under combined pure bending and traction

We analyze bone formation or resorption within a rectangular domain (fig. 3) corresponding to a biological situation pictured in fig. 2, relying on the field equations written in previous sections.

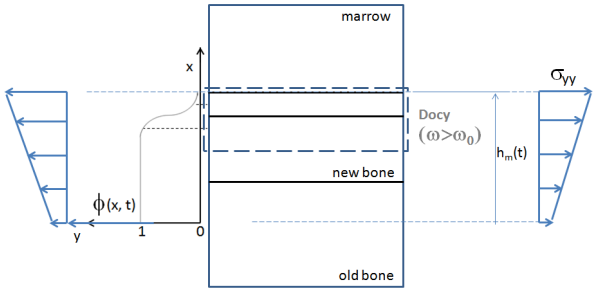

Figure 3: Mechanosensation of the mechanical stimulus by the osteocytes network (left). Schematics of the cortical bone RVE from fig. 2 with the motion of the diffuse interface (right).

The applied stress gradient associated to pure bending triggers internal stress and strain gradients within the domain show in fig. 3 (right), which will be unbalanced at the mesoscopic level of the RVE. The microstructure within the RVE (the stratified set of lamellae including the collagen fibers and microdamage) is also prone to strain gradient effects, thus its mechanical behavior is that of a strain gradient microcontinuum as well. This entails that a resulting strain continuum behavior will emerge at both microscopic and mesoscopic levels (the mesoscopic scale is the RVE scale). Accounting for the selected form of the stress field and assuming that $\sigma_{xx} = -p$ is uniform (corresponding to the boundary condition at the horizontal edge, $x = h_m(t)$), we assume the following form of Cauchy stress

$$\boldsymbol{\sigma} = \sigma_{xx}(y)\mathbf{e}_x \otimes \mathbf{e}_x + \sigma_{yy}(x)\mathbf{e}_y \otimes \mathbf{e}_y = -p\mathbf{e}_x \otimes \mathbf{e}_x + (\sigma_m + ax)\mathbf{e}_y \otimes \mathbf{e}_y \quad (40)$$

Using the equilibrium equation delivers the hyperstress tensor linear in x, $\mathbf{S} = Ax\mathbf{e}_y \otimes \mathbf{e}_y \otimes \mathbf{e}_x$, A=Cte. The elastic strain gradient tensor $\mathbf{k}_e$ generated by the bending load can be assimilated to the gradient of the elastic strain, viz

$$\boldsymbol{\varepsilon}_e = \frac{\sigma_{xx}}{E_x^{\,hom}}\mathbf{e}_x \otimes \mathbf{e}_x + \frac{\sigma_{yy}}{E_y^{\,hom}}\mathbf{e}_y \otimes \mathbf{e}_y$$
$$\rightarrow \mathbf{k}_e \cong \boldsymbol{\varepsilon}_e \otimes \nabla = \frac{a(t)}{E_y^{\,hom}}\mathbf{e}_y \otimes \mathbf{e}_y \otimes \mathbf{e}_x \quad (41)$$

for an orthotropic bone RVE with effective principal moduli $E_l^{\,hom} \cong 18\,\text{MPa}, E_t^{\,hom} \cong 10\text{MPa}$ in the longitudinal and transverse directions respectively (Reilly et al, 1975). Function a(t) in (47) has been introduced in (46). This leads to the order of magnitude of the curvature given by the ratio $a(t)/E_t^{\,hom}$; it further entails the hyperstress tensor using the strain gradient constitutive law for an assumed centrosymmetric RVE:

$$\mathbf{k}^e = \frac{a(t)}{E_y^{\,hom}}\mathbf{e}_y \otimes \mathbf{e}_y \otimes \mathbf{e}_x \Rightarrow \mathbf{S} = \left\{A_B^{\,hom}\right\}.\mathbf{k}^e \cong$$
$$\left(A_B^{\,hom}\right)_{yxyyyx}\frac{a(t)}{E_y^{\,hom}}\mathbf{e}_y \otimes \mathbf{e}_y \otimes \mathbf{e}_x \cong Ax\mathbf{e}_y \otimes \mathbf{e}_y \otimes \mathbf{e}_x \quad (42)$$
$$\Rightarrow A_B^{\,hom} = Ax\frac{E_y^{\,hom}}{a(t)}\mathbf{e}_y \otimes \mathbf{e}_y \otimes \mathbf{e}_x \otimes \mathbf{e}_y \otimes \mathbf{e}_y \otimes \mathbf{e}_x$$

The parameter A therein can be formally evaluated from the hyperstress tensor formally computed as the dyadic product of Cauchy stress with the spatial position within the RVE (Trinh, 2012), viz $\mathbf{S} = \frac{1}{|\text{RVE}|}\int_{\text{RVE}} \boldsymbol{\sigma} \otimes \mathbf{x}\,dV$, relying on numerical methods to evaluate previous volume integral. It is clear that the magnitude of parameter A in relation (42) depends on the internal lengths, elaborated as the ratio of the second gradient moduli to first gradient moduli. Note that the microscopic stress in previous integral should not be confused with the boundary mesoscopic stress over the RVE pictured on fig. 3; localizing the boundary stress uniformly within the RVE domain is a possible method used in the literature to identify the effective moduli, which however leads to a too soft response (Trinh et al., 2012).

An estimate of the internal length within cortical bone is given by the distance between two lamellae, of the order of $1 = 10\mu\text{m}$; it provides an estimate of the size of region over which second gradient effects are of importance and an estimate of the order of magnitude of the strain gradient moduli, here:

$$\left(A_B^{\,hom}\right)_{yxyyyx} = Ax\frac{E_y^{\,hom}}{a(t)}, l_i := \sqrt{A_B^{\,hom}/E} \cong 10\mu\text{m}$$
$$\Rightarrow A_B^{\,hom} = Ah_m(t)l_i^{\,2}\frac{E}{a(t)} \cong 100\text{N} \Rightarrow A = \frac{A_B^{\,hom}a(t)}{h_m(t)E^{hom}} \cong 2.10^4 \quad (43)$$

The effective first gradient modulus has been taken as the bulk modulus of bone, viz $E_s = 12$ GPa (Gibson, 2003); this is nevertheless an upper bound since the composite ultrastructure of lamellar cortical bone shall lead to a lower value, thus it is likely that parameter A (dimensionless) will take higher values. Referring to fig. 3, the mechanical boundary conditions write as follows:

$$\mathbf{u}(x=0,t) = \mathbf{0},\ \int_0^{h_m(t)} \mathbf{t}\,dx = F_x\mathbf{e}_x + F_y\mathbf{e}_y,\ \mathbf{t} = (\sigma_m + ax)\mathbf{e}_y \quad (44)$$

The first equality expresses the clamped bottom edge, the second and third ones the traction applied along the domain vertical edges (a unit thickness is considered here); a constant pressure is applied on the horizontal top edge, leading to an additional boundary condition that will however not be written. Consideration of the lateral boundary condition with previous chosen form of the stress component $\sigma_{yy}(x)$ leads to the expression of the interface height $h_m(t)$ versus time:

$$\mathbf{t} = \boldsymbol{\sigma}.\mathbf{n} - \text{div}(\mathbf{S}).\mathbf{n} \rightarrow \mathbf{t}(\mathbf{e}_y) = \{\sigma_m + (a(t) - A)x\}\mathbf{e}_y$$
$$\Rightarrow \int_0^{h_m(t)} \mathbf{t}.\mathbf{e}_y\,dx = F_y \Rightarrow h_m(t) = \frac{\left\{-\sigma_m + \left(\sigma_m^{\,2} + 2F_y(a(t) - 2A)\right)^{1/2}\right\}}{(a(t) - 2A)} \quad (45)$$

Thereby, a relation is obtained between the stress gradient parameter a(t) and the domain height $h_m(t)$, delimiting the border between the region of bone formation and marrow; previous relation clearly means that the stress gradient controls the speed of remodeling through the size of the grown domain and the hyperstress coefficient A. One recovers the expression of the interface height for the pure Cauchy continuum for a nil strain gradient coefficient A. The evolution of the interface height versus time for a linear temporal evolution $a(t) = a_0 + kt$ is pictured in fig. 4 for two opposite values of the 'slope' – parameter k- of function $a(t)$, resulting in two opposite situations of bone resorption and apposition respectively.

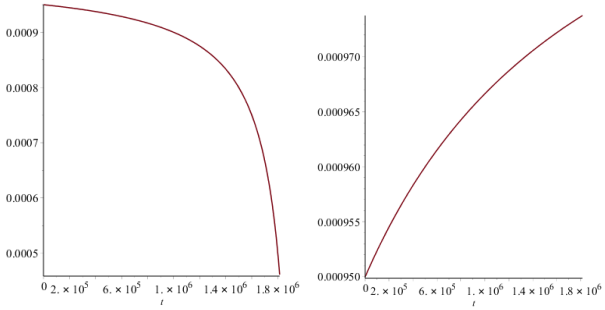

Figure 4: Evolution of the interface height (in meters) versus time (in seconds). Parameters values:
$a_0 = 10^{10}, F_y = 1000$ N, $\sigma_m = 1$MPa, A=2.10^6. Left:
$k = -5.10^3$, Right: $k = 5.10^3$

The strain gradient parameter A will strongly influence the response close when the denominator of previous expression of the interface height is close to the nil value: for a typical bone remodeling time of 21 days, this happens when $A = (a_0 + kT_{cycle})/2 = 4.64.10^8$ for the selected parameters set. Note also that parameter A may by itself change the sign of the factor $(a(t) - 2A)$ in the expression of the interface height, thus it controls the transition from bone apposition to bone resorption. Assuming as in (Ganghoffer et al., 2016) that the phase field contribution in Ginzburg-Landau equation vanishes in order to get a qualitative understanding of the RVE behavior

$$\alpha\Delta\phi + 2\phi(1-\phi)(2\phi - 1)W = 0 \quad (46)$$

the interface keeps a fixed shape over time, so that its shape is now determined by the sign of the quantity

$$6\phi\,(1-\phi)\left[-\frac{1}{2}\varepsilon^{e}:(C_B-C_M):\varepsilon^{e}-\frac{1}{2}k^{e}\right.$$
$$\left.\therefore A_B\,\therefore k^{e}+(\Psi_M-\Psi_B)\right]$$

which has to be evaluated at the position corresponding to the interface height. We quantify the effect of the elastic strain gradient energy to the elastic strain energy, evaluated for $x = h_m(t)$:

$$-\frac{1}{2}\boldsymbol{\varepsilon}_e:(\mathbf{C}_B-\mathbf{C}_M):\boldsymbol{\varepsilon}_e+\frac{1}{2}\mathbf{k}_e\,\therefore\mathbf{S}\cong\frac{1}{2}\left(\frac{\sigma_{xx}{}^2}{E_x^{\,hom}}+\frac{\sigma_{xx}{}^2}{E_y^{\,hom}}+Ax\frac{a(t)}{E_y^{\,hom}}\right)\quad(47)$$
$$\cong\frac{1}{2}\frac{p^2}{E_x^{\,hom}}+\frac{1}{2E_y^{\,hom}}\left(\frac{2F}{h_m(t)}-\sigma_m\right)^2+\frac{Ax}{2}\frac{a(t)}{E_y^{\,hom}}$$

Therefore, the strain gradient energy will enhance the total elastic strain energy by the additional positive term $\frac{Ax}{2}\frac{a(t)}{E_y^{\,hom}}$.

The ratio of second gradient to first gradient strain energy terms is evaluated based on the set of parameters used in fig. 4 and is plotted versus time in fig. 5 (it shall increase if the slope k is chosen to be positive instead). The second gradient energy is here smaller by a factor about 500 compared to the first gradient energy for the adopted values of the model parameters; the strain gradient has nevertheless via parameter A a strong influence on the bone remodeling process since it controls the transition from bone formation to resorption.

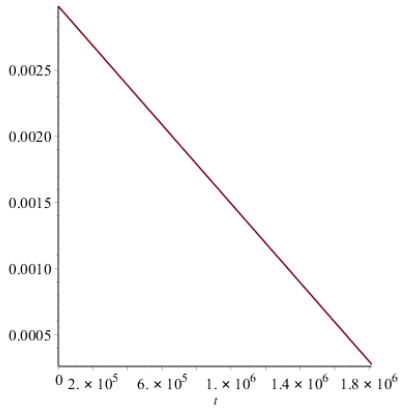

Figure 5: Evolution versus time of the ratio of second gradient to first gradient energy contributions in equ. (47). Parameter values: $a_0 = 10^{10}, F_y = 1000\text{N}, \sigma_m = 1\text{MPa}$, A=$2.10^6$, $k = -5.10^3$

6. Summary

We have developed a mechanobiological model of bone remodeling involving bone mineralization bone within a moving diffuse interface separating the marrow from newly formed bone. A phase field has been introduced, quantifying the degree of mineralization within the diffuse interface at the level of individual trabeculae; it varies continuously between the lower value (no mineral) and unity (fully mineralized phase corresponding to new bone). The model accounts for the strong strain gradients generated at the different scales of bone, caused by the curved interfaces prone to bending effects and the strong contrast of chemical composition and mechanical properties of the constituents. The biological basis is osteocytes being sensitive to the strain energy contribution including strain gradient terms that become pronounced close to the tip of microcrack. Since bone is a hierarchical structure, strain gradients exist at the different scale levels and propagate towards the higher scale levels; it is likely that the scale imbrication from the collagen molecule level to tissue level will lead to a whole spectrum of internal lengths the evaluation which is planned in future developments of the model.

Acknowledgements

Doctor Jessica Schiavi is financially supported by the Science Foundation Ireland (SFI) fund under Professor Laoise McNamara grant (14/IA/2884).

References

Ammar, K., B. Appolaire, G. Cailletaud, F. Feyel, S. Forest, 2009. Finite element formulation of a phase field model based on the concept of generalized stresses, Comp Mater Sci, 45, 800-805.

Bertram, J.E.A., A.A. Biewener, 1988. Bone curvature: Sacrificing strength for load predictability?, J. Theor. Biol., 131, 75-92.

Bonfoh, N., E. Novinyo, P. Lipinski, 2011. Modeling of bone adaptative behavior based on cells activities, Biomech. Model. Mechanobiol, 10, 789-798.

Buechner, P.M., R.S. Lakes, 2003. Size effects in the elasticity and viscoelasticity of bone, Biomech. Model. Mechanobiol, 1, 295-301.

Eremeyev, V.A., 2016. On effective properties of materials at the nano- and microscales considering surface effects, Acta Mech, 227, 29-42.

Forest, S., K. Ammar, B. Appolaire, Micromorphic vs. Phase-Field Approaches for Gradient Viscoplasticity and Phase Transformations, Springer Berlin Heidelberg, Berlin, Heidelberg, 2011, pp. 69-88.

Frasca, P., R. Harper, J.L. Katz, 1981. Strain and frequency dependence of shear storage modulus for human single osteons and cortical bone microsamples—Size and hydration effects, J. Biomech., 14, 679-690.

Ganghoffer, J.-F., R. Rahouadj, J. Boisse, S. Forest, Phase field approaches of bone remodeling based on TIP, Journal of Non-Equilibrium Thermodynamics, 2016, p. 49.

Giorgio, I., Andreaus, U., dell'Isola, F., & Lekszycki, T. Viscous second gradient porous materials for bones reconstructed with bio-resorbable grafts. Extreme Mechanics Letters, 2017, 13, 141-147.

Gurtin, M.E., A. Ian Murdoch, 1975. A continuum theory of elastic material surfaces, Arch. Ration. Mech. Anal., 57, 291-323

Harrigan, T.P., M. Jasty, R.W. Mann, W.H. Harris, 1988. Limitations of the continuum assumption in cancellous bone, J. Biomech., 21, 269-275.

Kennedy, O.D., B.C. Herman, D.M. Laudier, R.J. Majeska, H.B. Sun, M.B. Schaffler, 2012. Activation of resorption in fatigue-loaded bone involves both apoptosis and active pro-osteoclastogenic signaling by distinct osteocyte populations, Bone, 50, 1115-1122.

Komarova, S.V., R.J. Smith, S.J. Dixon, S.M. Sims, L.M. Wahl, 2003. Mathematical model predicts a critical role for osteoclast autocrine regulation in the control of bone remodeling, Bone, 33, 206-215.

Lakes, R., 1995. On the torsional properties of single osteons, J. Biomech., 28, 1409-1410

Martin, R.B., D.B. Burr, N.A. Sharkey, Skeletal tissue mechanics, Springer1998.

Mindlin, R.D., 1964. Micro-structure in linear elasticity, Arch. Ration. Mech. Anal., 16, 51-78.

Nowak, M., J. Sokołowski, A. Żochowski, 2018. Justification of a certain algorithm for shape optimization in 3D elasticity, Struct Multidiscipl Optim, 57, 721-734.
O'Brien, F.J., D. Taylor, T. Clive Lee, 2005. The effect of bone microstructure on the initiation and growth of microcracks, J. Orth. Res., 23, 475-480.
Park, H.C., R.S. Lakes, 1986. Cosserat micromechanics of human bone: Strain redistribution by a hydration sensitive constituent, J. Biomech., 19, 385-397.
Ramézani, H., A. El-Hraiech, J. Jeong, C.-L. Benhamou, 2012. Size effect method application for modeling of human cancellous bone using geometrically exact Cosserat elasticity, Comput Method Appl M, 237-240, 227-243.
Reilly, D.T., A.H. Burstein, 1975. The elastic and ultimate properties of compact bone tissue, J. Biomech., 8, 393-405.
Sciarra, G., F. dell'Isola, O. Coussy, 2007. Second gradient poromechanics, Int J Solids Struct, 44, 6607-6629.
Steigmann, D., R. Ogden, Plane deformations of elastic solids with intrinsic boundary elasticity, Proceedings of the Royal Society of London A: Mathematical, Physical and Engineering Sciences, The Royal Society, 1997, pp. 853-877.
Steigmann, D., R. Ogden, Elastic surface—substrate interactions, Proceedings of the Royal Society of London A: Mathematical, Physical and Engineering Sciences, The Royal Society, 1999, pp. 437-474.
Trinh, D.K., R. Janicke, N. Auffray, S. Diebels, S. Forest, 2012. Evaluation of generalized continuum substitution models for heterogeneous materials, 10, 527-549.
van der Linden, J.C., D.H. Birkenhäger-Frenkel, J.A.N. Verhaar, H. Weinans, 2001. Trabecular bone's mechanical properties are affected by its non-uniform mineral distribution, J. Biomech., 34, 1573-1580.
van Eijden, T.M.G.J., L.J. van Ruijven, E.B.W. Giesen, 2004. Bone Tissue Stiffness in the Mandibular Condyle is Dependent on the Direction and Density of the Cancellous Structure, Calcif. Tissue Int., 75, 502-508.
Vaughan, T.J., C.T. McCarthy, L.M. McNamara, 2012. A three-scale finite element investigation into the effects of tissue mineralisation and lamellar organisation in human cortical and trabecular bone, J Mech Behav Biomed Mater, 12, 50-62.
Webster, D., F.A. Schulte, F.M. Lambers, G. Kuhn, R. Müller, 2015. Strain energy density gradients in bone marrow predict osteoblast and osteoclast activity: A finite element study, J. Biomech., 48, 866-874.